



# Effect of particle size and co-deposition technique on hardness and corrosion properties of Ni–Co/SiC composite coatings

Babak Bakhit, Alireza Akbari \*

Surface Engineering Group, Advanced Materials Research Center, Faculty of Materials Engineering, Sahand University of Technology, P.O. Box 51335-1996, Tabriz, Iran

## ARTICLE INFO

### Article history:

Received 18 January 2012

Accepted in revised form 29 May 2012

Available online 4 June 2012

### Keywords:

Ni–Co/SiC composite coatings

Nanocomposite coatings

Sediment co-deposition

Microhardness

Corrosion resistance

## ABSTRACT

Ni–Co/SiC alloy matrix composite coatings were electrodeposited in a modified Watt's bath containing micro and nano sized SiC particles by using conventional electro-co-deposition (CECD) and sediment co-deposition (SCD) techniques. The deposits were characterized using SEM, EDX and XRD analyses, and microhardness and potentiodynamic polarization measurements. The maximum incorporation of the SiC micro- and nano-particles was obtained using the SCD technique at deposition current densities of 2 and 3 A/dm<sup>2</sup>, respectively. It was found that in the composite coatings, incorporation of SiC particles improves the microhardness of unalloyed Ni and Ni–Co alloy matrices. The nanocomposite coatings exhibit higher microhardness values than microcomposite ones. The potentiodynamic polarization measurements in 3.5% NaCl solution revealed that the corrosion resistance of the Ni–Co/SiC nanocomposite coatings is much higher than the Ni–Co alloy and Ni–Co/SiC microcomposite coatings. Moreover, corrosion resistance of Ni–Co/SiC nanocomposite coatings deposited by SCD technique is higher than the ones deposited by CECD technique. Corrosion resistance of the studied Ni–Co/SiC composite coatings was considerably affected by Co content, SiC particle size and content. Hardness enhancement was related to the structural features, and corrosion behavior was discussed based on the formation of corrosion micro cells, diminishing the effective metallic area, and increasing and hindering the corrosion paths.

© 2012 Elsevier B.V. All rights reserved.

## 1. Introduction

Many attempts have been made to find methods for enhancing the surface properties of metal components to protect against corrosion and wear and reducing their costs since all of them are the effective factors in the degradation of industrial parts. Electro-deposition is considered as one of the most important and cost effective industrial techniques for producing protective coatings. It is conducted at normal pressure and ambient temperatures and provides high deposition rate and high throwing power. Electro-deposition of Ni and Ni-alloy coatings has found widespread use in many industrial fields [1,2]. Compared to Ni coatings, Ni based composite coatings provide superior mechanical properties and higher corrosion and wear resistances [3]. Therefore, the interest for electro-deposition of Ni based composite coatings has increased due to their excellent properties.

Composite electro-deposition is a method of codepositing insoluble particles suspended in an electrolyte with metallic cations. Over the past decades, successful co-deposition of different types of particles such as oxide [4–6], carbide [7,8], polymer [9,10], nitride [11,12], diamond [13], graphite [14] and metallic [15] particles has been reported. Among the various composite coating systems produced by

combination of different matrix and reinforcement materials, Ni/SiC composite coatings have been investigated extensively [8,16,17] for exploring the impact of the co-deposition conditions and the properties of the deposited coatings. Adjusting electro-deposition parameters can improve the properties of composite coatings [18]. Recently, more attention has been focused on the synthesis of composite coatings by co-deposition of reinforcing particles in the alloy matrices like Ni–W [19], Zn–Ni [20,21], Ni–Fe [22] and particularly Ni–Co alloys [23–25]. However, only few investigations have been made for the electro-deposition of Ni–Co/SiC nanocomposite coatings [25–29].

One of the great interests in the synthesis of composite coatings is the higher values of incorporated particles. The extent of the particle incorporation not only depends on the deposition parameters such as electrolyte composition, pH values, presence of additives, deposition current type and density, but is also greatly influenced by the co-deposition technique. Sediment co-deposition (SCD) technique is an effective method to increase the particle incorporation [14,30]. Unlike the conventional electro-co-deposition (CECD) technique, in the SCD technique the electrodes are set horizontally in the electrolyte. In the CECD technique particles are suspended in the electrolyte under continuous stirring, but in the SCD technique periodic stirring is applied to allow particles to be suspended in the electrolyte and sediment on the cathode. Therefore, the gravity force provides additional tendency for particle settling in the SCD technique.

\* Corresponding author. Tel.: +98 412 3459416; fax: +98 412 3444333.  
E-mail address: [akbari@sut.ac.ir](mailto:akbari@sut.ac.ir) (A. Akbari).

Limited data is available in literature concerning the effect of SiC particle size and co-deposition technique on the properties of Ni-Co/SiC composite coatings [25–29]. Corrosion behavior of composite coatings has been studied extensively [4,8,30–34]. Many published reports have usually focused only on determination of the corrosion rate of electrodeposited composite coatings [4,31–33]. However, a complete understanding of how the microstructural features in conjunction to the various deposition parameters are affected by the corrosion behavior and corrosion mechanisms requires more detailed studies.

In the present work, the CECD and SCD techniques have been applied for electro-deposition of Ni-Co/SiC composite coatings in a modified Watt's bath containing SiC micro- and nano-particles. The Ni-Co alloy was chosen as the matrix material as it has been previously reported to possess promising properties for Ni-Co alloy coatings [35–37]. The effects of particle size, co-deposition technique and deposition current density were investigated on microhardness and corrosion resistance of composite coatings. The goal was to produce Ni-Co/SiC composite coatings with higher microhardness and corrosion resistance.

## 2. Experimental

Electro-deposition of Ni-Co/SiC composite coatings was carried out in a modified Watt's bath by adding SiC micro- and nano-particles to the electrolyte using two different techniques; (i) the CECD technique wherein electrodes were set vertically in the electrolyte and (ii) the SCD technique wherein electrodes were set horizontally in the electrolyte. During the deposition process, the electrolyte was magnetically stirred at 350 rpm agitation rate. Electrolyte stirring was performed continuously in the CECD technique and intermittently in the SCD technique with 10 s resting time after each 300 s stirring time. The schematic illustration of the CECD and SCD setups used in this work is shown in Fig. 1.

The electro-deposition bath was prepared using Merck analytical grade reagents and contained 250 g/l of  $\text{NiSO}_4 \cdot 6\text{H}_2\text{O}$ , 50 g/l of  $\text{CoSO}_4 \cdot 7\text{H}_2\text{O}$ , 40 g/l of  $\text{NiCl}_2 \cdot 6\text{H}_2\text{O}$ , 40 g/l of  $\text{H}_3\text{BO}_3$ , 0.35 g/l of  $\text{NaC}_{12}\text{H}_{25}\text{SO}_4$  and 5 g/l of SiC particles. In preliminary studies, a SiC bath concentration of 5 g/l and a pH of 4.3 were determined as optimum conditions leading to the maximum incorporation of the SiC nanoparticles in the deposited coatings. The micro and nano sized SiC particles used in this study had an average particle size of 20 nm and 10  $\mu\text{m}$ , respectively. The utilized SiC particles had high purity (>99%) and were manufactured by Plasmachem GmbH of Germany. The coatings were deposited on copper plate substrates as cathode and a pure nickel was used as anode by employing

a DC power supply at various current densities (1–4  $\text{A}/\text{dm}^2$ ). The distance between the anode and the cathode was 3 cm. The temperature of the bath was maintained at 45 °C. The pH was adjusted by  $\text{H}_2\text{SO}_4$  and NaOH at around 4.3.

The copper substrates (cathodes) were mechanically polished with silicon carbide abrasion papers and ultrasonically cleaned in ethanol and acetone for 10 min, sequentially and washed in distilled water after the cleaning process. The substrates were activated in 10%  $\text{H}_2\text{SO}_4$  for 60 s before final use. Prior to deposition, the electrolyte containing particles were alternatively subjected to ultrasound waves produced using a Hielscher-UP100H disperser and vigorous magnetic agitation (~700 rpm) using a magnetic stirrer for 24 h before electro-deposition to achieve a highly uniform dispersion of particles. The agitation started by a 60 minute ultrasonic dispersion followed by repeated cycles of a 315 minute magnetic stirring and a 30 minute ultrasonic dispersion (during 24 h), and the last step was the ultrasonic dispersion. After deposition, in terms of removing loosely adsorbed particles from the cathode surface, the coatings were ultrasonically cleaned in the distilled water for 5 min after the electro-deposition process. The deposition time was adjusted to attain a coating thickness of around 30  $\mu\text{m}$ .

The surface morphology and cross section of the composite coatings was investigated by using a CamScan MV2300 scanning electron microscope (SEM). An Oxford Energy Dispersive X-ray detector (EDX) coupled to SEM was utilized to determine the chemical analysis and SiC content of the coatings. Five randomly chosen areas were analyzed (at 500 $\times$  magnification) and an average value was calculated. Standard deviation of five independent measurements is reported as error bars. The phase structure, average grain size and preferred orientation of coatings were determined from XRD patterns recorded in the Bragg–Brentano configuration using a D8 ADVANCE-BRUKER AXS X-ray diffractometer operated at 40 keV and 40 mA with the  $\text{Cu-K}\alpha$  radiation ( $\lambda = 1.5406 \text{ \AA}$ ). Integral peak width was used to estimate the crystallite size of the coatings after excluding the instrumental broadening. Instrumental broadening was determined from the XRD pattern of a standard  $\text{LaB}_6$  sample. The preferred orientation was evaluated by calculation of the texture coefficient. The microhardness of the coatings was measured using a MDPEL-M400 GL microhardness tester equipped with a Vickers indenter under indenting load and time of 50 g and 10 s, respectively. Hardness measurements were performed on the polished cross-section and top surface of the coatings. An average of ten different measurements from the top of each deposit was reported as coating microhardness.

Potentiodynamic polarization measurements were used to investigate the corrosion resistance of composite coatings. Electrochemical measurements were carried out in the non-aerated 3.5% NaCl corrosive medium using an EG&G-Parstat 2263 potentiostat/galvanostat system. A saturated calomel electrode (SCE) was used as the reference electrode and a platinum electrode with an exposed area of about 10 times larger than the working electrode was used as the counter electrode. Potentiodynamic sweeping was performed in the potential range of  $\pm 250 \text{ mV}$  with respect to  $E_{ocp}$  by 1 mV/s sweeping rate. The corrosion current density of the deposits was calculated using the Stern–Geary equation from the polarization measurement.

## 3. Results and discussion

### 3.1. Electro-deposition

Fig. 2 illustrates the effect of deposition current density on the SiC micro- and nano-particle content in the Ni-Co/SiC composite coatings deposited by SCD technique. For a given amount of particle concentration (5 g/l SiC), SiC nano-particle content in the deposits is increased with increasing deposition current density and reaches to a maximum value at 3  $\text{A}/\text{dm}^2$ . SiC nano-particle content is decreased at the higher deposition current densities. The same trend is observed for the

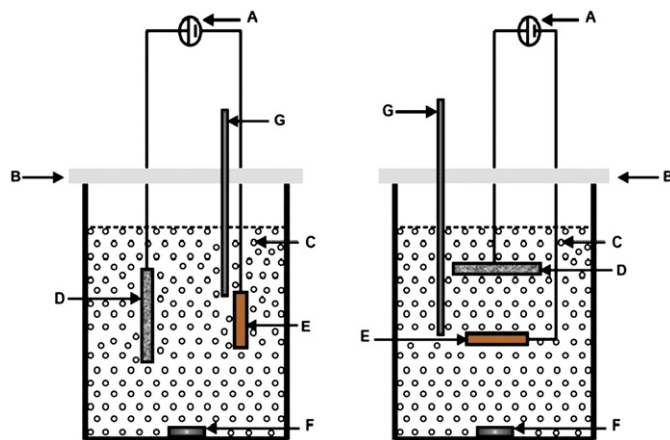


Fig. 1. Schematic image of the co-deposition setups; (A) DC power supply, (B) Epoxy cover, (C) SiC particles, (D) anode, (E) cathode, (F) magnetic bar and (G) external pH-temperature probe.

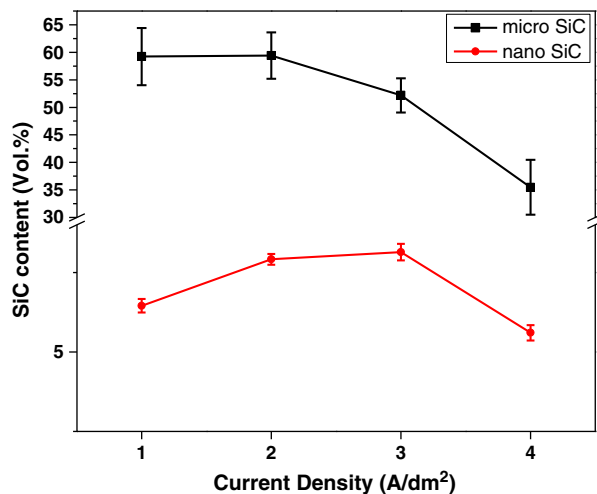


Fig. 2. Effect of the deposition current density on the SiC micro- and nano-particle content in Ni-Co/SiC composite coatings deposited by SCD technique (5 g/l of SiC).

Ni-Co/SiC microcomposite coatings despite the fact that the highest amount of SiC micro-particles in these coatings is achieved at a deposition current density of 2 A/dm<sup>2</sup>.

The rate of film growth, and therefore volume percent of the incorporated reinforcing particles, is determined by the relative magnitudes of the rates by which the particles and cations arrived to the growing film surface. Increasing deposition current density may enhance both rates. At the constant electrolyte agitation rate, increasing the deposition current density up to a maximum value leads to an enhanced transfer of charged particles inside the electrolyte, thereby, increasing the particle adsorption on the cathode surface. In contrast, further increase of deposition current density results in more rapid deposition of metallic cations compared to particle incorporation due to their rapid transfer in the electrolyte. Therefore, higher deposition current densities are caused to decrease particle content in the deposits. These observations are in close agreement with previously reported results for co-deposition of different types of particles [15,32,33] and SiC micro- and nano-particles embedded in metal and alloy matrices [38–40].

According to Fig. 2, the SiC micro-particle content in Ni-Co/SiC composite coatings is higher than the SiC nano-particle content in the entire studied range of deposition current densities. This is due to the fact that large particles settle down more rapidly than small particles under the positive effects of gravity force in the SCD technique. It can be seen that the largest amount of SiC micro- and nano-particles in the Ni-Co/SiC composite coatings (59.4 vol.% and 8.1 vol.%) was achieved at the deposition current densities of 2 A/dm<sup>2</sup> and 3 A/dm<sup>2</sup>, respectively.

In order to capture the effects of the co-deposition technique on the SiC particle incorporation, electro-deposition of Ni-Co/SiC nanocomposite coatings was carried out by using two different SCD and CECD co-deposition techniques. Fig. 3 shows the variation of SiC nano-particle content as a function of the deposition current density for both co-deposition techniques. The SiC nano-particle content for the coatings deposited by CECD technique as a function of the deposition current density varies in a similar trend from those deposited by SCD technique and reaches to a maximum at 3 A/dm<sup>2</sup>. However, Fig. 3 indicates that the percentage of embedded SiC nano-particles is higher for the SCD technique. Here it can also be correlated to the positive effects of gravity force on sedimentation of SiC nano-particles on the growing film surface in the SCD technique.

Fig. 4 shows a schematic image of the applied forces to an immersed particle inside the hydrodynamic and concentration boundary layers in the electrolyte regardless of agitation forces. In the SCD technique, both

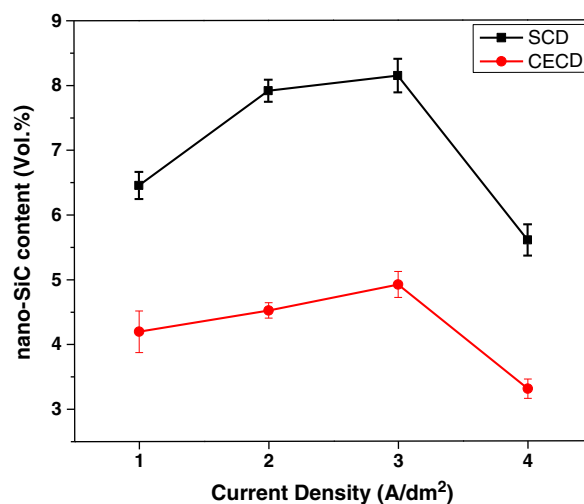


Fig. 3. Effect of the deposition current density on particle content in Ni-Co/SiC nanocomposite coatings deposited by CECD and SCD techniques (5 g/l of nano-SiC).

the gravitational and electrophoretic forces act vertically in the same direction while in the CECD technique, the electrophoretic force acts horizontally and perpendicularly to the gravitational force. The alignment of these forces in the SCD technique enhances the SiC nano-particle incorporation by their facilitated settling down. As it is mentioned above, this effect is more influential in the case of coarser particles, because the frictional drag forces become smaller for larger particles by dwindling the surface/volume ratio; therefore, it is expected that incorporation of SiC micro-particles is higher than the SiC nano-particles. Frictional drag force increases with decreasing particle size.

### 3.2. Characterization of deposited coatings

#### 3.2.1. Phase structure

The X-ray diffraction (XRD) patterns of Ni-45 wt.% Co alloy and Ni-Co/SiC composite coatings are indicated in Fig. 5. These XRD patterns illustrate that the matrix of the composite coatings is composed of a Ni-Co solid solution with a face centered cubic (fcc) structure. Also, calculation of the texture coefficient reveals dominance of a (111) preferred orientation. Incorporation of SiC micro- and nano-particles does not change neither the phase structure nor the preferred orientation of the Ni-Co alloy matrix since unreinforced Ni-45 wt.% Co alloy coatings exhibit a fcc structure with a (111) preferred orientation. However, incorporation of SiC particles in both composite coatings

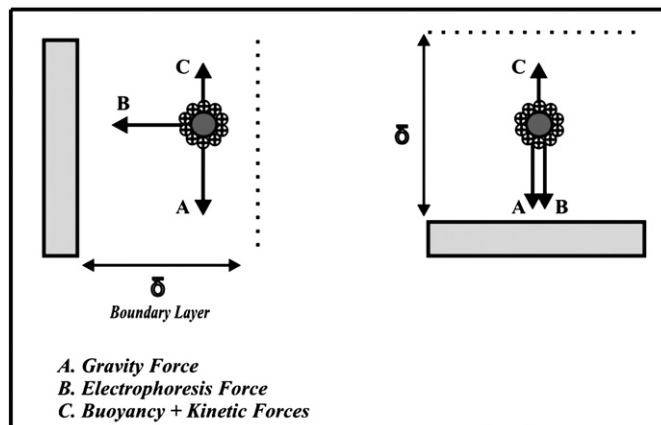
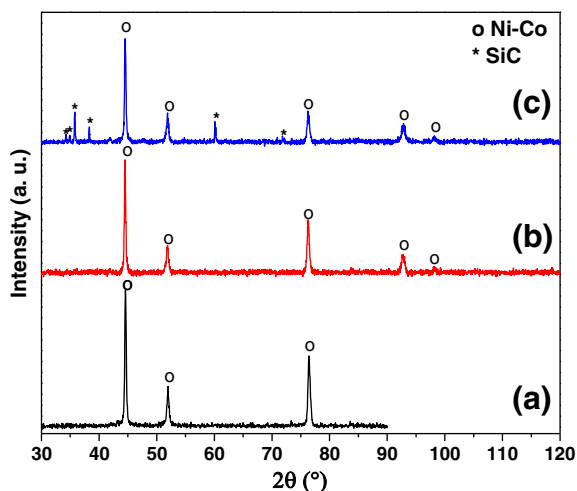


Fig. 4. Schematic image of the applied forces for an immersed particle.



**Fig. 5.** X-ray diffraction patterns of (a) Ni-45 wt.% Co alloy, (b) microcomposite and (c) nanocomposite coatings deposited by using SCD technique (5 g/l SiC and 2 A/dm<sup>2</sup>).

leads to a slight decrease in the intensity of the matrix peaks. Reduction in the intensities of the matrix (i.e. Ni–Co alloy) peaks in the diffraction patterns of microcomposite coatings is stronger than the nanocomposite coatings. In addition, the XRD pattern of the microcomposite coating contains several peaks at the 2θ angles of 34°, 35.73°, 38.24°, 41.5°, 60.2° and 73.59° which respectively corresponded to the (101), (102), (103), (104), (110) and (203) reflections of the SiC phase with a hexagonal close-packed (hcp) structure. The absence of the SiC peaks in the XRD pattern of the nanocomposite coating is due to the low amount (~7.9 vol.%) and small size (~20 nm) of SiC nano-particles.

### 3.2.2. Surface morphology

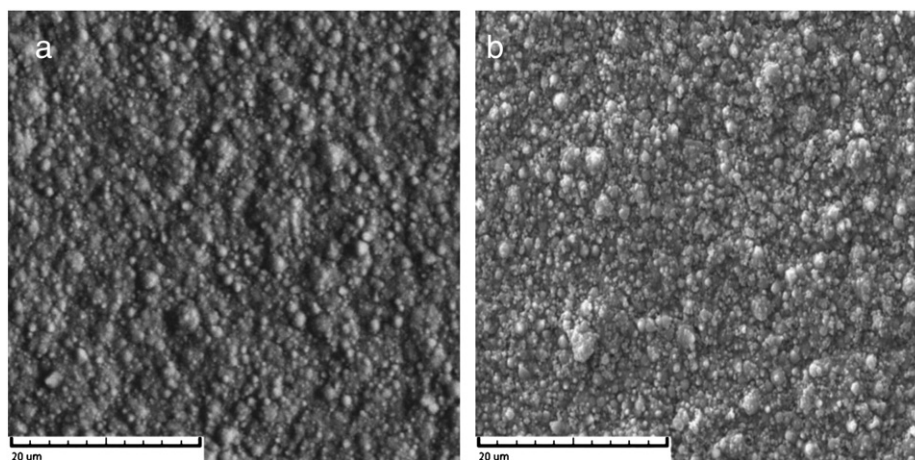
In order to observe the effects of particle size and co-deposition technique on the distribution of SiC particles and surface morphology of coatings, the surface morphology of the deposits was studied using SEM observations. Fig. 6. illustrates the surface morphologies of the Ni-45 wt.% Co alloy coating and Ni-Co/SiC nanocomposite coating containing 8.1 vol.% SiC nano-particles electrodeposited at the same electro-deposition conditions (in the modified Watt's bath with and without SiC nano-particles). Both coatings are characterized by nodular morphology. Compared to the Ni-45 wt.% Co alloy coating,

the nodule size of the nanocomposite coating is decreased due to the incorporation of SiC nano-particles into the Ni–Co alloy matrix.

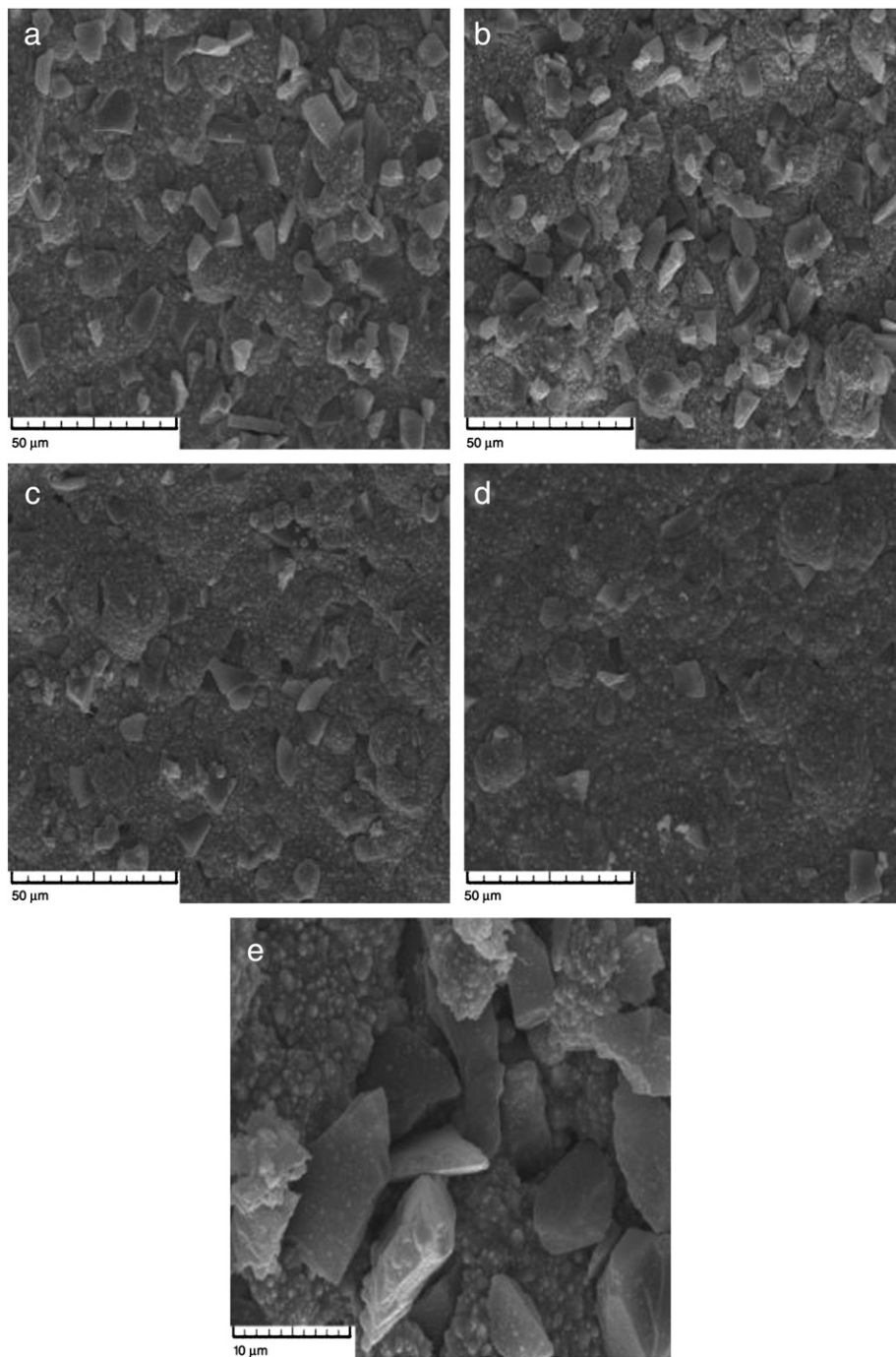
The effect of the deposition current density on the surface morphology of Ni–Co/SiC microcomposite coatings deposited by SCD technique is shown in Fig. 7. The utilized SiC micro-particles have a non-spherical shape with an average particle size of 10 μm. This figure confirms the descending effect of the deposition current density on the incorporation of micro-SiC particles. Besides, the large number of micro-SiC particles was not completely entrapped in the matrix (Fig. 7e) and micro voids are visible around some particles which are not filled by the matrix alloy. This is due to the rapid incorporation of the SiC micro-particles with respect to the reduction rate of metallic cations (Ni<sup>2+</sup> and Co<sup>2+</sup>) in the SCD technique. As it is shown in Fig. 7a and b, SiC micro-particles have accumulated throughout the surface of the microcomposite coatings. Higher incorporation of SiC micro-particles generates a “shadowing” effect and leaves unfilled regions in the shadowed areas. In fact, there is not enough time to complete the filling of the micro void surrounding particles by metallic cations. Moreover, the Si mapping images (Fig. 8) reveal that the SiC micro-particles have a rather uniform distribution in the matrix. The Si content is decreased in the mapping images of microcomposite coatings by increasing the deposition current density. Fig. 9 shows the surface morphologies and Si mapping images of microcomposite and nanocomposite coatings deposited by SCD technique. It can clearly be seen that distribution of SiC particles in the Ni–Co matrix is uniform for both coatings.

Fig. 10 shows the surface morphology of the Ni–Co/SiC nanocomposite coatings deposited by SCD and CECD techniques versus the deposition current density. During co-deposition, agglomerates form by coalescence of the SiC nano-particles mainly due to their higher surface activity [41]. From Fig. 10 it is observed that surface morphologies of Ni–Co/SiC nanocomposite coatings deposited by SCD and CECD techniques are similar and the agglomerated SiC nano-particles are distributed uniformly in the Ni–Co alloy matrix. Meanwhile, the number density of the agglomerated SiC nano-particles in the SCD technique is higher than in the CECD technique. In addition, the number of agglomerated particles in the coatings deposited using current densities of 1 and 4 A/dm<sup>2</sup> is lower than those deposited at current densities of 2 and 3 A/dm<sup>2</sup>. Therefore, changing the co-deposition technique from CECD to SCD helps to achieve a higher incorporation and a uniform distribution of agglomerated SiC nano-particles in the Ni–Co alloy matrix.

SEM image from the cross sectional microstructure of the nanocomposite coatings is shown in Fig. 11. This figure indicates a porosity free structure with a uniform distribution of the SiC nano-particle agglomerates in the Ni–Co matrix. Uniformity of thickness and good



**Fig. 6.** Surface morphology of (a) Ni-45 wt.% Co alloy and (b) Ni-Co/SiC nanocomposite coatings (5 g/l of SiC and 3 A/dm<sup>2</sup>).



**Fig. 7.** Surface morphology of Ni-Co/SiC microcomposite coatings deposited by SCD technique and deposition current densities of (a)  $1/\text{dm}^2$ , (b)  $2/\text{dm}^2$ , (c)  $3/\text{dm}^2$ , and (d)  $4/\text{dm}^2$  and (e) a high magnification image of (b) ( $5\text{ g/l}$  of micro-SiC).

adherence to the substrate are also observed. To verify composition uniformity across the coating thickness, the line scans of the Ni, Co, Si and Cu elements are shown on the cross sectional SEM image (Fig. 12). Fairly uniform distributions for Ni and Co and a quite uniform distribution for elemental Si and therefore SiC nano-particles are obtained.

The EDX spectra of the Ni-Co/SiC composite coatings deposited by SCD technique in the electrolyte containing  $5\text{ g/l}$  of SiC micro- and nano-particles are shown in Fig. 13. The Si peak intensity in the EDX spectra of the microcomposite coating is significantly higher than the nanocomposite coating and consequently the intensity of the Ni and Co peaks is lower for the microcomposite coating. From the presented results, it is confirmed that the amount of SiC micro-particles is much higher than the amount of SiC nano-particles in the Ni-Co alloy matrix.

In addition, the amount of nickel and cobalt in the microcomposite coating is lower than the nanocomposite coating; it is due to a more rapid incorporation of SiC micro-particles compared to the reduction rate of metallic cations.

The surface morphology of Ni-Co/SiC microcomposite coatings deposited by SCD and CECD techniques is illustrated in Fig. 14. It is seen that the amount of SiC micro-particles in coating deposited by CECD technique is much lower than that in the coating deposited by SCD technique.

### 3.2.3. Microhardness

Fig. 15 compares the effects of deposition current density on the microhardness of Ni-Co/SiC microcomposite and nanocomposite

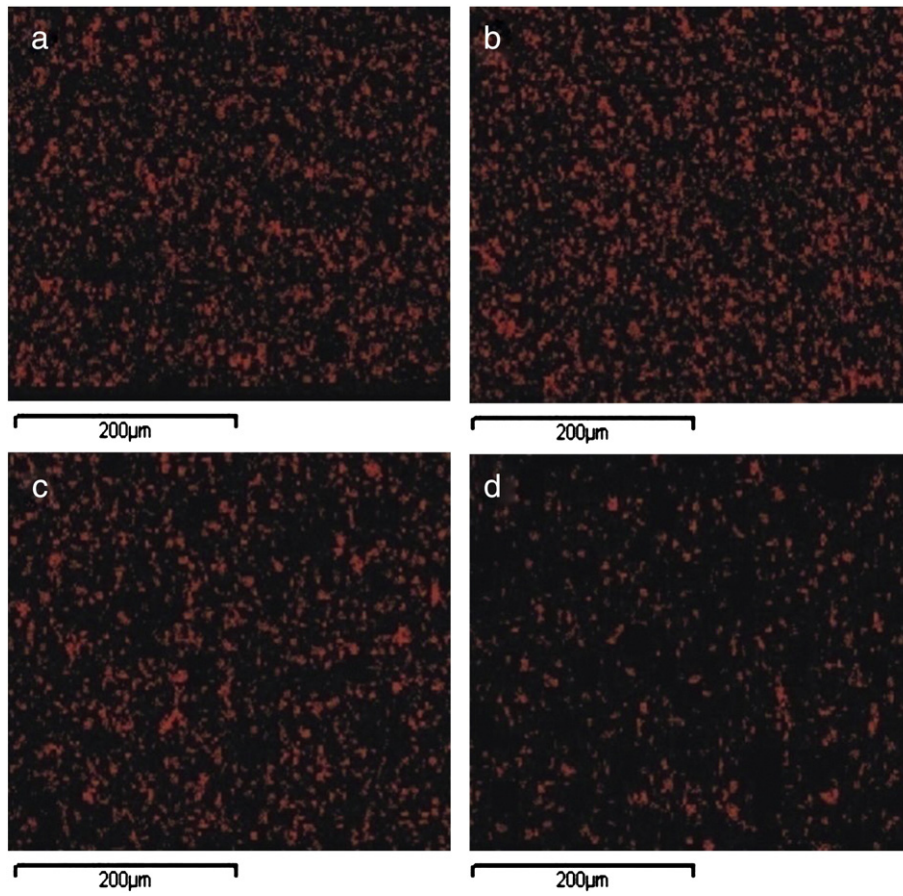


**Fig. 8.** Si mapping images of the Ni-Co/SiC microcomposite coating surface deposited by SCD technique and deposition current densities of (a) 1 A/dm<sup>2</sup>, (b) 2 A/dm<sup>2</sup>, (c) 3 A/dm<sup>2</sup> and (d) 4 A/dm<sup>2</sup> (5 g/l of micro-SiC).

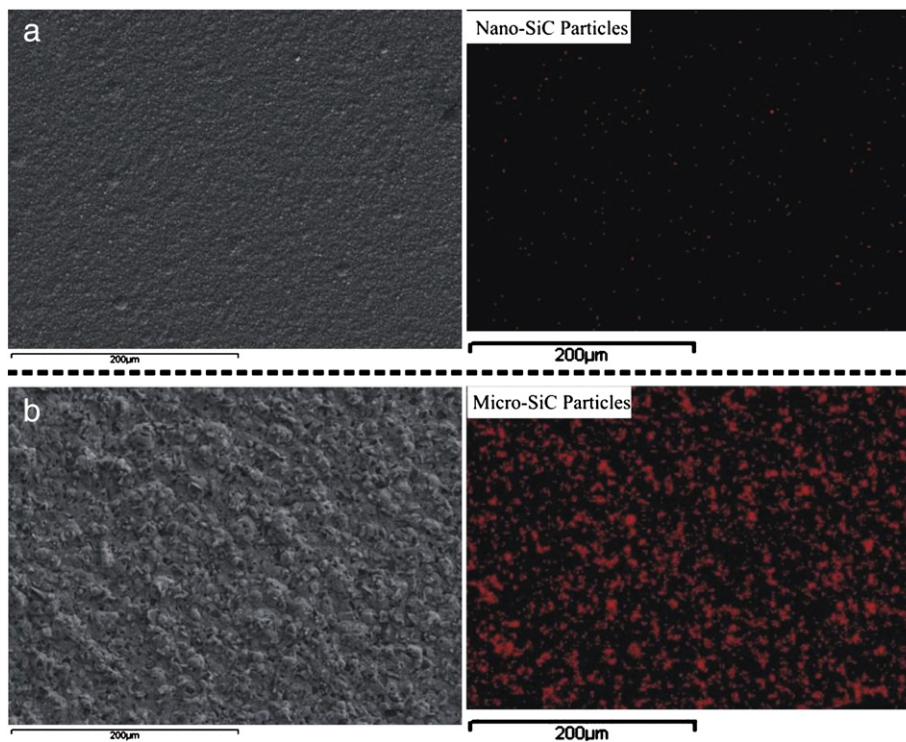


**Fig. 9.** Surface morphology and Si mapping image of (a) the nanocomposite coating and (b) the microcomposite coating deposited by SCD technique (5 g/l of SiC and 2 A/dm<sup>2</sup>).

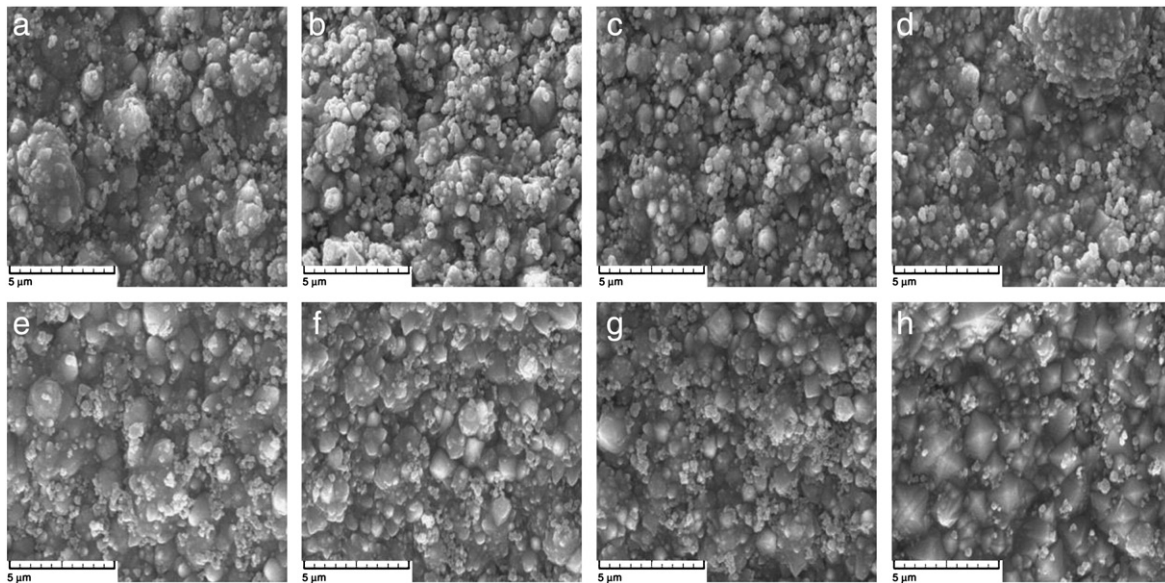


**Fig. 10.** Surface morphology of Ni–Co/SiC nanocomposite coatings deposited by current densities of (a) 1 A/dm<sup>2</sup>, (b) 2 A/dm<sup>2</sup>, (c) 3 A/dm<sup>2</sup>, and (d) 4 A/dm<sup>2</sup> by SCD technique and (e) 1 A/dm<sup>2</sup>, (f) 2 A/dm<sup>2</sup>, (g) 3 A/dm<sup>2</sup>, and (h) 4 A/dm<sup>2</sup> by CECD technique (5 g/l of nano-SiC).

coatings deposited by SCD technique. The microhardness of the composite coatings is initially enhanced by increasing the deposition current density, and becomes maximum at 3 A/dm<sup>2</sup>. This behavior is similar for two kinds of composite coatings, but the microhardness of the nanocomposite coatings is higher than the microcomposite ones in the studied range of deposition current density. Comparison of Figs. 2 and 15 indicates that in the nanocomposite coatings, variations in both microhardness and SiC nano-particle content with deposition current density resemble together, but in the microcomposite coatings the microhardness variation does not follow the same trend as the variation of the SiC micro-particle content with deposition current density.

According to Fig. 15, the highest microhardness of the Ni–Co/SiC microcomposite coatings is obtained for coatings deposited by using a deposition current density of 3 A/dm<sup>2</sup>, although the SiC micro-particle content of this coating (52.2 vol.%) is lower than the coatings deposited by using deposition current densities of 1 and 2 A/dm<sup>2</sup> (59 vol.% and 59.4 vol.%, respectively). It is more probably related to the existence of micro voids in the structure of Ni–Co/SiC

microcomposite coatings. As is shown in Fig. 7, the number of micro voids in the microcomposite coatings decreases by increasing the deposition current density. The probability of micro void formation during the co-deposition of composite coatings increases, especially when the particles are agglomerated [42]. Furthermore, formation of micro voids diminishes the coating microhardness. Therefore, it can be concluded that porous structure formation is the main reason for lower microhardness of Ni–Co/SiC microcomposite coatings.

Fig. 16 illustrates the effect of the co-deposition technique on the microhardness of Ni–Co/SiC nanocomposite coatings versus the deposition current density. The microhardness variation versus the deposition current density has a similar trend for both co-deposition techniques, since a decline in microhardness of coatings arises after reaching the maximum value at a deposition current density of 3 A/dm<sup>2</sup>. On the other side, the microhardness of the Ni–Co/SiC nanocomposite coatings deposited by SCD technique is higher than those deposited by CECD technique in the studied range of deposition current density. It can be correlated to a higher incorporation of SiC nano-particles in the SCD technique (see Fig. 3).

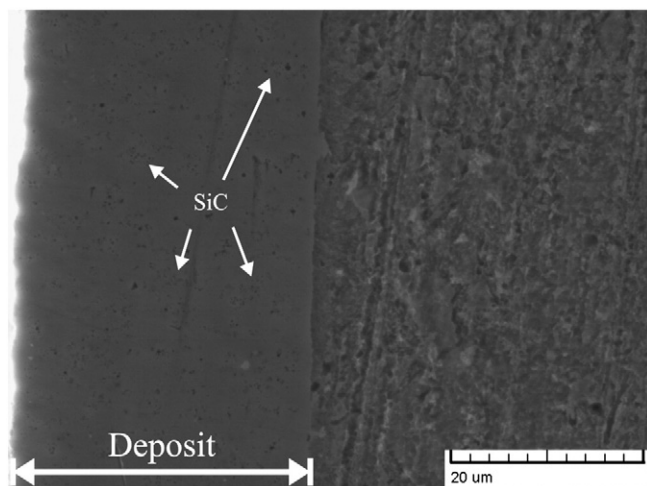


**Fig. 11.** Cross-section of the Ni–Co/SiC nanocomposite coating (5 g/l of nano-SiC and 3 A/dm<sup>2</sup>).

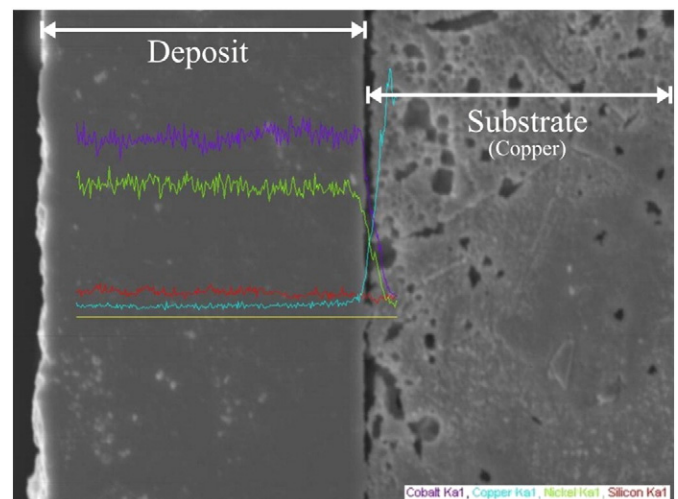


**Fig. 12.** Line scan element curves of the Ni–Co/SiC nanocomposite coating (5 g/l of nano-SiC and 2 A/dm<sup>2</sup>).

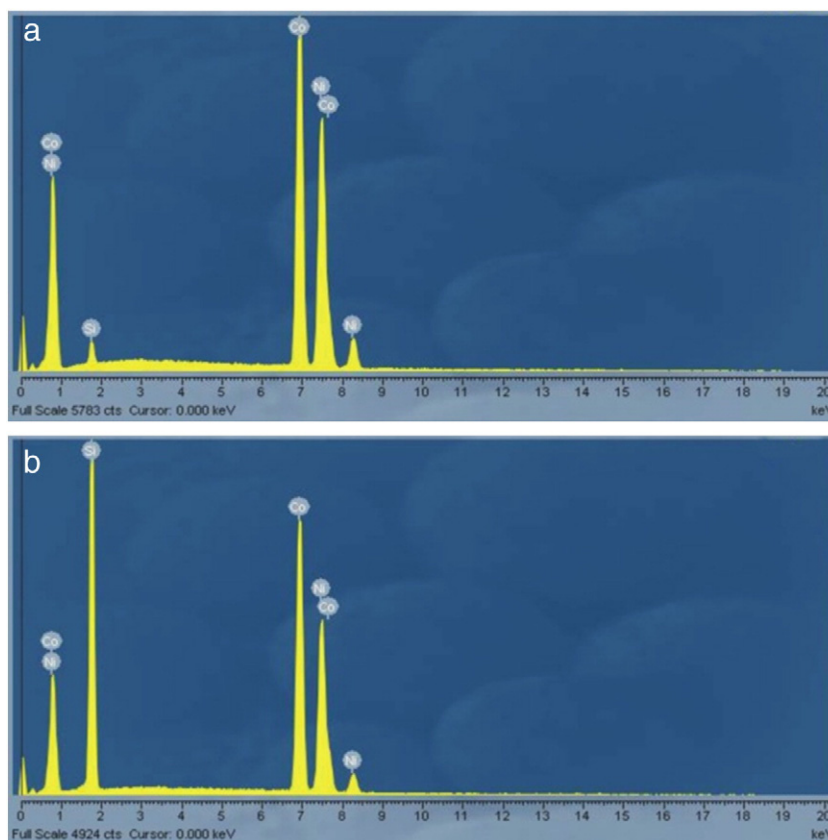


Fig. 13. EDX spectra of (a) the nanocomposite coating and (b) the microcomposite coatings deposited by using the SCD technique (5 g/l of SiC and 3 A/dm<sup>2</sup>).

The microhardness of the composite coatings is determined by the properties of the reinforcing particles and matrix material. According to the basic understandings on plastic deformation mechanisms, hardening mechanisms of alloy matrix composite coatings are significantly associated with (i) solid solution hardening by choosing an alloyed matrix, (ii) grain refinement of the matrix, (iii) texture evolution and (iv) reinforcing phase induced hardening [43–45].

Microhardness of unalloyed Ni, Ni–45 wt.% Co alloy and Ni–Co/SiC composite coatings deposited by SCD technique is compared in Fig. 17. This figure indicates that the microhardness of the composite coatings is improved through the incorporation of SiC particles in the Ni–Co matrix, however, alloying of Ni with 45 wt.% Co has drastically enhanced its hardness. Therefore, as indicated in Fig. 17 and reported in previous studies the microhardness of the Ni–Co alloy coatings is higher than the unalloyed Ni coatings [35,42]. Thus, a part of microhardness enhancement in the Ni–Co/SiC composite coatings is related to the higher microhardness of the Ni–Co matrix compared to the unalloyed Ni matrix due to formation of substitutional solid solution.

Investigations have shown that the incorporation of reinforcing particles promotes the nucleation rate and demotes the grain growth [8,44,46]. Reduction of the matrix grain size is an effective way in order to increase the microhardness of composite coatings, according to the Hall–Petch relation [47,48]. To explore the role of grain refinement, the grain size of different Ni, Ni–45 wt.% Co, and Ni–Co/SiC metallic and nanocomposite coatings, all deposited under similar conditions, is depicted in Fig. 18. Measured grain sizes are calculated from the XRD peak width broadening analysis using the (200) matrix alloy peak. Comparing the grain size of different coatings according to Fig. 18, indicates that: (i) Co plays a significant role in grain size reduction of the unalloyed Ni coating, as fivefold smaller grain sizes are obtained for the Ni–45 wt.% Co alloy coating with respect to the unalloyed Ni coating, (ii) incorporation of the SiC micro and nano-particles in the Ni–Co/SiC composite coatings does not affect the grain size of the Ni–Co matrix.

These results indicate that the smaller grain sizes of the Ni–Co/SiC nanocomposite coatings compared to the unalloyed Ni coating are due to the alloying with Co rather than the incorporation of the SiC micro- and nano-particles.

Zimmerman et al. [45] reported higher and lower microhardness values for nanocrystalline Ni coatings with (111) and (200) preferred orientations, respectively. However in the present study a considerable change in the preferred orientation of the matrix phase was not observed.

In the conventional ex-situ metal matrix composites where the average size of the reinforcing phase and matrix grains are in the range of a few microns to tens of microns, the plastic deformation of the composite is governed and entirely controlled by the dislocation activity. The strengthening contribution of the reinforcing (ceramic) particles takes place according to the Orowan mechanism, as the matrix carries the load and the embedded particles impede the mobility of the dislocations. In the studied Ni–Co/SiC nanocomposite coatings, while the agglomeration of the reinforcing SiC nano-particles takes place in some extent, the average grain size of the matrix alloy and the average size of the un-agglomeration particles are around 20 nm. When the grain size becomes less than a certain value in the nano range (20–50 nm), the grains become free from dislocation and the conventional dislocation mediated plastic deformation becomes hindered [48,49]. For the electrodeposited pure coatings, the grain size at which the grains become free from dislocations is reported to be around 20 nm [50]. For the Ni–Co alloy matrix this grain size is estimated to be slightly smaller than the unalloyed Ni. At the small sizes where the grains become free from dislocations, it is expected that the contribution of the grain boundary mediated processes in plastic deformation becomes comparable with the dislocation based mechanisms or even dominant. In nanocrystalline materials grain boundaries act as dislocation sources and generate complete or partial dislocations that they slide freely inside the grains until they meet the opposing grain boundary, which

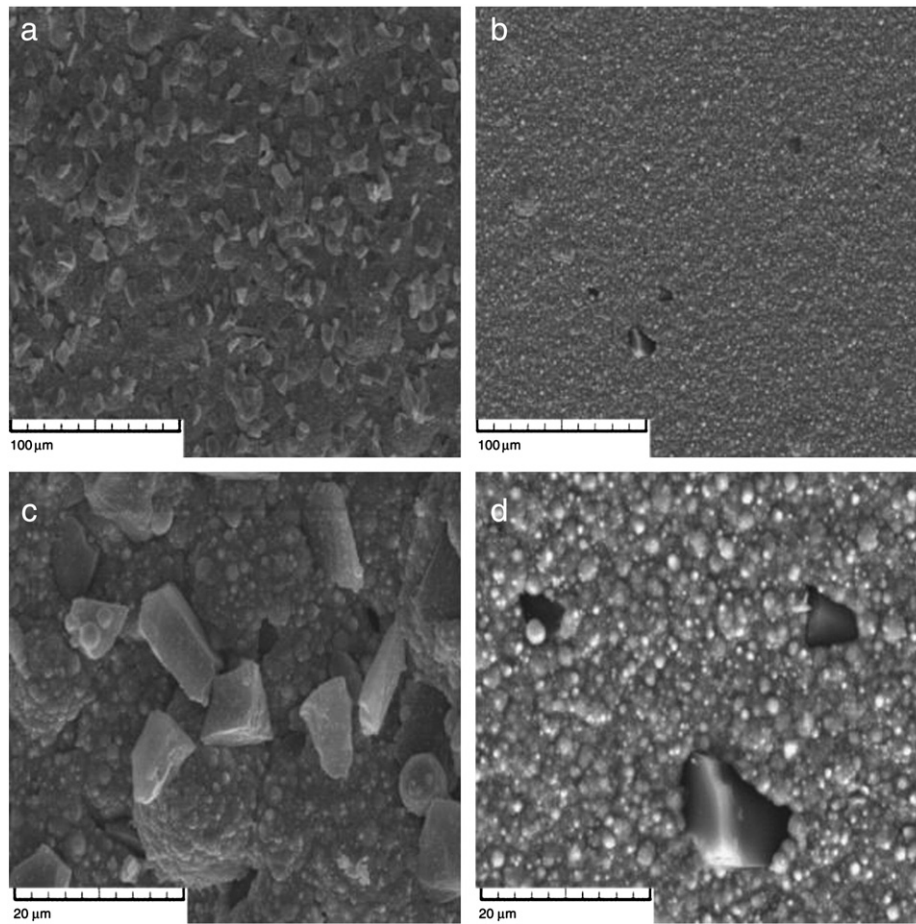


Fig. 14. Surface morphology of the Ni-Co/SiC microcomposite coatings deposited by (a, c) SCD technique and (b, d) CECD technique (5 g/l of micro-SiC and 2 A/dm<sup>2</sup>).

acts as a sink [48]. Grain boundary mediated plastic deformation processes take place through several ways such as grain boundary sliding, coble creep and grain rotation [51]. The incorporated SiC particles may be beneficial in preventing grain boundary sliding, however this needs to be verified in future studies.

According to Fig. 18 the average grain size of the matrix in the nanocomposite coating is about 20 nm which is comparable with

the average size of the non-agglomerated SiC nano-particle. This size is about 25 nm in the microcomposite coating which is very small compared to the 10 μm average size of the SiC micro-particles. Therefore, in the studied composite coatings, SiC micro- and nano-particles or their agglomerates cannot be embedded entirely inside the matrix grains; instead they could be surrounded by several grains. The majority of the SiC nano-particles, except the non-agglomerated

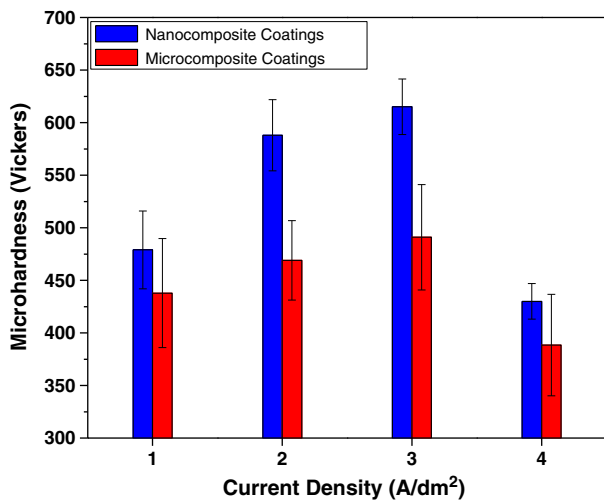


Fig. 15. Effect of the deposition current density on the microhardness of the Ni-Co/SiC microcomposite and nanocomposite coatings deposited by using the SCD technique (5 g/l of SiC).

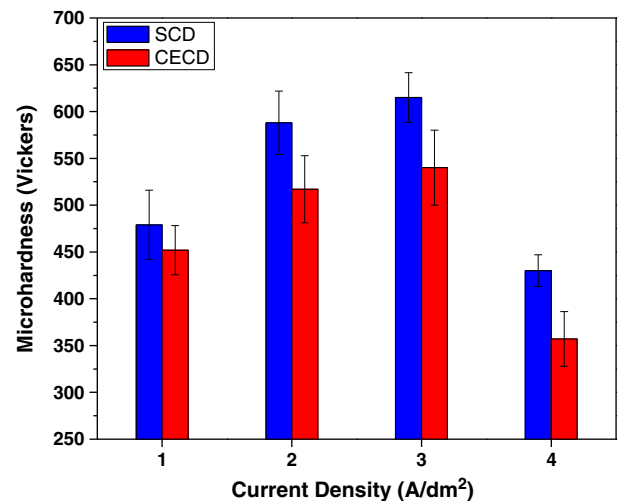


Fig. 16. Effect of the co-deposition technique on the microhardness of the Ni-Co/SiC nanocomposite coatings versus the deposition current density (5 g/l of nano-SiC).

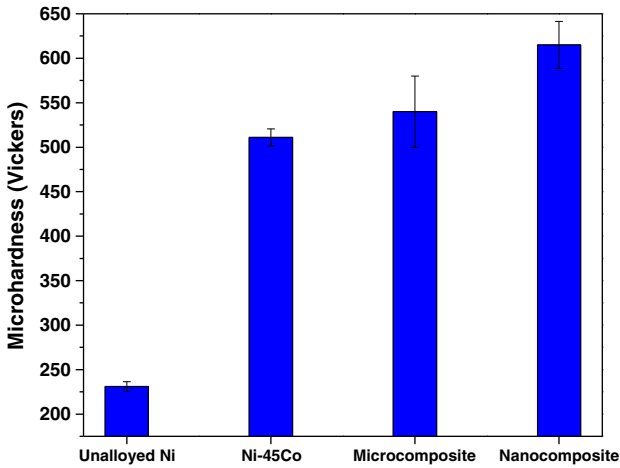


Fig. 17. Microhardness of unalloyed Ni, Ni–45 wt.% Co and Ni–Co/SiC composite coatings deposited by SCD technique (5 g/l of SiC and 3 A/dm<sup>2</sup>).

particles which are smaller than 20 nm, and all of the SiC micro-particles are embedded as inter-crystalline phase. Consequently some matrix grain boundaries are replaced with particle–matrix interfaces. At these interfaces, the SiC micro- and nano-particles can strengthen the boundaries and hinder the plastic deformation. It is expected that in comparable amount of the embedded SiC particles as the number density of the nano-particles is much higher than the micro-particles their contribution to the strengthening will be greater than the micro-particles.

The above discussions indicate that while the presence of the SiC micro- and nano-particles enhances hardness of the composite coatings, the strengthening mechanisms are quite different compared to the conventional dispersion and Orowan hardenings.

3.2.4. Corrosion properties

The potentiodynamic polarization curves of the Ni–45 wt.% Co alloy coating and Ni–Co/SiC composite coatings, determined in the 3.5% NaCl corrosive medium, are presented in Fig. 19. The results of the potentiodynamic polarization measurements are summarized in Table 1. The reported corrosion current densities were calculated by

using the Stern–Geary equation from the polarization measurements [52]:

$$i_{corr} = \frac{\beta_a \cdot \beta_c}{2.303 \times R_p (\beta_a + \beta_c)} \tag{1}$$

where  $i_{corr}$  is the corrosion current density,  $R_p$  is the polarization resistance, and  $\beta_a$  and  $\beta_c$  are the anodic and cathodic Tafel slopes, respectively. Also, the polarization resistance ( $R_p$ ) was calculated by following the equation:

$$R_p = \left. \frac{dE}{di} \right|_{E=E_{ocp}} \approx \frac{E}{i} \tag{2}$$

There is no existence of a passivation plateau for the Ni–45 wt.% Co alloy coating and Ni–Co/SiC microcomposite coating, nevertheless the Ni–Co/SiC nanocomposite coating exhibits an unstable passivation behavior and a small active–passive transition peak by anodic polarization. Based on the extracted data from the polarization curves, the Ni–Co/SiC nanocomposite coating has the highest corrosion potential ( $E_{corr}$ ), whereas the Ni–45 wt.% Co alloy coating has the lowest corrosion potential. The corrosion current density ( $i_{corr}$ ) of the Ni–Co/SiC microcomposite coating is much lower than the Ni–45 wt.% Co alloy coating. Besides, the corrosion current density ( $i_{corr}$ ) of the Ni–Co/SiC nanocomposite coating is lower than the Ni–Co/SiC microcomposite coating and it has a higher corrosion resistance ( $R_p$ ), which implies that the corrosion rate of the Ni–Co/SiC nanocomposite coating is lower than the corrosion rate of the Ni–45 wt.% Co alloy and Ni–Co/SiC microcomposite coatings.

To compare the effect of the co-deposition technique on the corrosion resistance of Ni–Co/SiC nanocomposite coatings, potentiodynamic polarization measurements were performed in the 3.5% NaCl corrosive medium. The potentiodynamic polarization curves of the Ni–Co/SiC nanocomposite coatings deposited by CECD and SCD techniques and their electrochemical data are given in Fig. 20 and Table 2, respectively. According to Fig. 20, the polarization curve of the nanocomposite coating deposited by SCD technique is shifted to lower current densities and positive potentials. The data in Table 2, indicates that the Ni–Co/SiC nanocomposite coating deposited by SCD technique exhibits a higher corrosion potential ( $E_{corr}$ ), lower corrosion current density ( $i_{corr}$ ) and higher corrosion resistance ( $R_p$ ) than the Ni–Co/SiC nanocomposite coating deposited by CECD technique. This may be related to a higher incorporation of SiC nano-particles in the SCD technique (see Fig. 3).

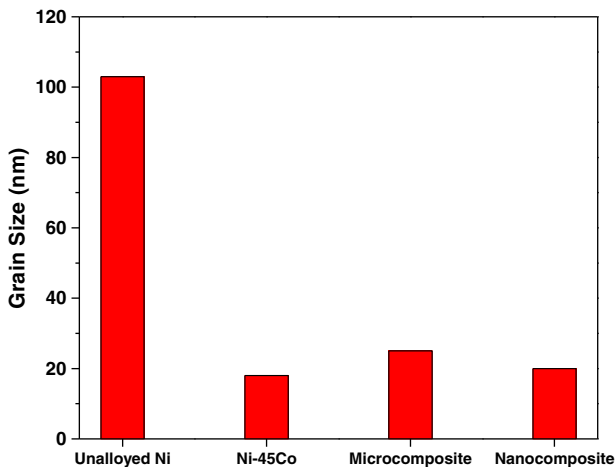


Fig. 18. The grain size of unalloyed Ni, Ni–45 wt.% Co and Ni–Co/SiC composite coatings deposited by SCD technique (5 g/l of SiC and 3 A/dm<sup>2</sup>).

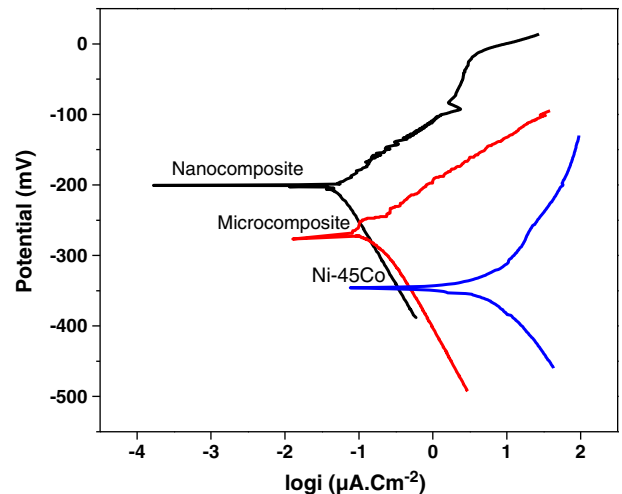


Fig. 19. The potentiodynamic polarization curves of Ni–45 wt.% Co alloy coating and Ni–Co/SiC composite coatings deposited by using the SCD technique.

**Table 1**

Electrochemical results of the potentiodynamic polarization curves of Ni–45 wt.% Co alloy coating and Ni–Co/SiC composite coatings deposited by using SCD technique.

| Coating        | Co (wt.%) | SiC (vol.%) | $E_{ocp}$ (mV) | $\beta_a$ (mV/dec) | $\beta_c$ (mV/dec) | $E_{corr}$ (mV) | $i_{corr}$ ( $\mu\text{A}\cdot\text{cm}^{-2}$ ) | $R_p$ ( $\text{k}\Omega\cdot\text{cm}^2$ ) |
|----------------|-----------|-------------|----------------|--------------------|--------------------|-----------------|---|--|
| Ni–Co          | 45        | Zero        | –346           | 177.26             | 120.9              | –354            | 6.57  | 4.75                                       |
| Microcomposite | 38        | 52.2        | –277           | 71.94              | 162.1              | –257            | 0.137   | 158.48                                     |
| Nanocomposite  | 55        | 8.1         | –201           | 71.18              | 176.5              | –199            | 0.050   | 439.46                                     |

Therefore, it is concluded that changing the co-deposition technique is an effective method to enhance the corrosion resistance of Ni–Co/SiC nanocomposite coatings.

It is well established that the corrosion mechanism of composite coatings differs from common metallic coatings. Several influential factors justify the corrosion resistance of such coatings, including production process, properties of both matrix and reinforcing phases, and their interface and service conditions.

The matrix role on corrosion resistance of composite coatings significantly relates to the matrix chemical composition, grain size, phase structure and preferred orientation. The corrosion resistance of Ni–Co alloy coatings is a result of simultaneous effects of some detrimental and beneficial factors. Alloying can affect the corrosion resistance by changing the nobility of materials [53]. It is expected that the electrochemical activity of Ni–Co alloys is greater than the electrochemical activity of unalloyed Ni by increasing the cobalt content, since cobalt is a more active element than nickel [54]. On the other hand, in the Ni–Co/SiC composite coatings, incorporation of SiC particles is enhanced by increasing the cobalt concentration in the electrolyte that it can be an effective factor to improve the corrosion resistance of Ni–Co/SiC composite coatings [38]. Thus, cobalt has two distinct effects on the corrosion resistance of Ni–Co/SiC composite coatings; a detrimental direct effect (decreasing the nobility of Ni–Co alloys) and a beneficial indirect effect (increasing the incorporation of SiC particles).

One of the effective factors on the corrosion resistance of metallic coatings might be the density of grain boundaries. It was found that corrosion process proceeds along the grain boundaries and exacerbates by increasing the grain boundary density [55]. The grain boundaries due to their higher energy are more susceptible to corrosion attacks compared to the inter-crystalline parts of the material. Hence, a decrease of grain size (increase of the grain boundary density) leads to a decrease of corrosion resistance. As a result, amorphous materials exhibit a better corrosion resistance than polycrystalline materials due to lack of grains and grain boundary [56]. Since the grain boundaries are prone to corrosion attacks and no passive film forms on the

common Ni–Co alloy coatings, hence, at the cobalt contents higher than the critical value, the corrosion resistance of Ni–Co alloy coatings is decreased by increasing the cobalt content due to the decrease of the grain size [42,55]. It was confirmed that single phase structures are more corrosion resistant than two-phase structures. Besides, the fcc structures due to their higher packing factor compared with bcc structures have a higher corrosion resistance [37]. A part of the corrosion resistance of the studied composite coatings can be linked to their phase structure as the matrix of the composite coatings exhibited a single phase fcc structure.

Effects of reinforcing particles on the corrosion resistance of composite coatings might be associated with several factors such as particle size, particle content, uniform distribution of particles, diminishing the effective metallic area, formation of micro-galvanic cells, acting of particles as inert physical barriers to the corrosion initiation and growth of corrosion products, extending and hindering the corrosion paths, filling the micro holes and submicron defects during electro-deposition.

The first effect of reinforcing particles on the corrosion behavior of composite coatings is the reduction of the effective metallic area exposed to the corrosive medium [8]. The SiC particles are naturally semi-conductor and act as inert physical barriers. Hence, if the SiC particles are uniformly distributed in the metallic matrix, the effective area exposed decreases and the corrosion potential shifts to more noble values.

In the previous studies on corrosion resistance of composite coatings, it has been established that the preferential corrosion attacks occur at the interface of the reinforcing particles and matrix due to the formation of micro-galvanic cells, which is caused to change the corrosion mechanism from localized corrosion and/or pitting corrosion to uniform corrosion [34]. The SiC particles act as cathode and the Ni–Co alloy matrix acts as anode in the Ni–Co/SiC composite coatings immersed in the corrosive medium, because the standard potential of the SiC particles is more positive than the Ni–Co alloy matrix. T. Lampke et al. [57] indicated that the depth of pits on the surface of composite coatings exposed to the NaCl corrosive medium is lower than the metallic coatings. The reinforcing particles act as a barrier to further the propagation of pits and preferential sites for pitting initiation are the matrix areas adjacent to the particle–matrix interface and not the interface itself. However, in the discontinuous and porous interfaces, the corrosive ions (such as  $\text{Cl}^-$  ions in salt solutions) can diffuse along interfaces and deteriorate the corrosion resistance.

Since the electro-deposition usually is associated with the formation of crevices, gaps and porosities, incorporation of reinforcing particles can occupy these defects during co-deposition. The size of these defects is approximately submicron and micron. Hence, the SiC nano-particles smaller than 100 nm can easily fill these defects compared with the micro-SiC particles [40]. This modifying effect of the SiC nano-particles improves the corrosion resistance through the filling corrosion attack zones on the coating surface. SEM cross-section images of the studied Ni–Co/SiC nanocomposite coatings do not exhibit porosities at higher magnifications that it confirms the useful effect of SiC nano-particles to reduce corrosion rate. Moreover, as is shown in Fig. 7, the porous structure of the microcomposite coatings is the main weakness of these coatings against corrosion attacks.

Regarding the above discussions, the corrosion resistance of the Ni–Co/SiC composite coatings is associated with several interrelated microstructural parameters. Consequently, the observed passivation behavior for the nanocomposite coating may be explained by the

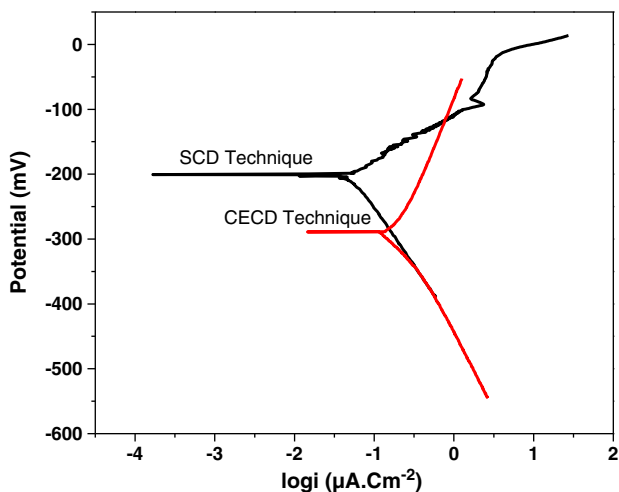


**Fig. 20.** The potentiodynamic polarization curves of the Ni–Co/SiC nanocomposite coatings deposited by using CECD and SCD techniques (5 g/l of nano-SiC and 3 A/dm<sup>2</sup>).

**Table 2**

Electrochemical results of Ni–Co/SiC nanocomposite coatings potentiodynamic polarization curves versus co-deposition technique.

| Co-deposition technique | Co (wt.%) | SiC (vol.%) | $E_{ocp}$ (mV) | $\beta_a$ (mV/dec) | $\beta_c$ (mV/dec) | $E_{corr}$ (mV) | $i_{corr}$ ( $\mu\text{A}\cdot\text{cm}^{-2}$ ) | $R_p$ ( $\text{k}\Omega\cdot\text{cm}^2$ ) |
|-------------------------|-----------|-------------|----------------|--------------------|--------------------|-----------------|---|--|
| SCD                     | 55        | 8.1         | –201           | 71.18              | 176.5              | –199            | 0.050   | 439.46                                     |
| CECD                    | 59.6      | 4.9         | –289           | 250.1              | 172.2              | –297            | 0.168   | 262.20                                     |

formation of an unstable protective film. Indeed, a higher density of grain boundaries and particle/matrix interfaces and also, the formation of micro-galvanic cells result in the formation of a layer of corrosion products which acts as a protective film.

#### 4. Conclusions

Ni–Co/SiC microcomposite and nanocomposite coatings were electrodeposited using conventional (CECD) and sediment (SCD) co-deposition techniques in a modified Watt's bath and the effects of SiC particle size and co-deposition techniques on the microhardness and corrosion resistance of composite coatings were investigated. Based on the obtained results the following conclusions can be made:

1. Incorporation of SiC micro-particles (max. 59.4 vol.%) into the composite coatings was much higher than the SiC nano-particles (max. 8.1 vol.%) in the SCD technique. In addition, incorporation of SiC micro- and nano-particles using the SCD technique was higher than the CECD technique.
2. SEM studies revealed a dense and porosity free structure for the nanocomposite coating whereas a porous and micro-voided structure for the microcomposite coatings. Micro void density in microcomposite coatings strongly depends on the SiC micro-particle volume fraction which is closely correlated to the deposition technique.
3. The microhardness of the Ni–Co/SiC microcomposite and nanocomposite coatings was higher than the unalloyed Ni and Ni–Co alloy coatings. The majority of the SiC nano-particle and all of the SiC micro-particle are embedded as inter-crystalline phase. A higher microhardness of composite coatings confirmed the combined strengthening effects of matrix grain refinement and reinforcing induced by the hard SiC phase at the grain boundaries.
4. The microhardness of the nanocomposite coatings was found to be greater than the microcomposite coatings in different deposition current densities, despite their lower volume fraction of SiC phase. Also, nanocomposite coatings deposited by SCD technique exhibit higher microhardness values than nanocomposite coatings deposited by CECD technique due to the incorporation of SiC nano-particles in higher extents.
5. Potentiodynamic polarization studies indicated that the corrosion resistance of the Ni–Co/SiC composite coatings was much better than the Ni–Co alloy coatings. The better corrosion resistance of the composite coatings was discussed based on the cobalt content, SiC particle content, formation of corrosion micro cells, diminishing of the effective metallic area, and increasing and hindering of the corrosion paths.
6. Nanocomposite coatings exhibited a higher corrosion resistance compared with microcomposite coatings. The lower corrosion resistance of the microcomposite coatings is related to the existence of micro voids and porosities in their structure.

#### References

- [1] T. Burakowski, Surface Engineering of Metals; Principles, Equipment, Technologies, Translated by W. K. Liliental, CRC Press, 1999.
- [2] D. Golodnitsky, Y. Rosenberg, A. Ulus, Electrochim. Acta 47 (2002) 2707.
- [3] A. Brenner, Electro-deposition of Alloys Principles and Practice, Academic Press, 1963.

- [4] A.C. Ciubotariu, L. Benea, M. Lakatos-Varsanyi, V. Dragan, Electrochim. Acta 53 (2008) 4557.
- [5] X.S. Liang, J.H. Ouyang, Y.F. Li, Y.M. Wang, Appl. Surf. Sci. 255 (2009) 4316.
- [6] W. Wang, F.Y. Hou, H. Wang, H.T. Guo, Scr. Mater. 53 (2005) 613.
- [7] Y. Boonyongmaneerat, K. Saengkiattiyut, S. Saenapitak, S. Sangsuk, Surf. Coat. Technol. 203 (2009) 3590.
- [8] I. Garcia, A. Conde, G. Langelaan, J. Fransaeer, J.P. Celis, Corros. Sci. 45 (2003) 1173.
- [9] Z. Abdel Hamid, I.M. Ghayad, Mater. Lett. 53 (2002) 238.
- [10] P. Bercot, E. Pena-Munoz, J. Pagetti, Surf. Coat. Technol. 157 (2002) 282.
- [11] E. Pompei, L. Magagnin, N. Lecis, P.L. Cavallotti, Electrochim. Acta 54 (2009) 2571.
- [12] A.A. Aal, M. Bahgat, M. Radwan, Surf. Coat. Technol. 201 (2006) 2910.
- [13] M. Pushpavanam, H. Manikandan, K. Ramanathan, Surf. Coat. Technol. 201 (2007) 6372.
- [14] A. Afshar, M. Ghorbani, M. Mazaheri, Surf. Coat. Technol. 187 (2004) 293.
- [15] I.N. Bilnik, A. Budniok, B. Losiewicz, L. Pajak, E. Lagiewka, Thin Solid Films 474 (2005) 146.
- [16] H.K. Lee, H.Y. Lee, J.M. Jeon, Surf. Coat. Technol. 201 (2007) 4711.
- [17] P. Gyftou, E.A. Pavlatou, N. Spyrellis, Appl. Surf. Sci. 254 (2008) 5910.
- [18] W. Pilth, Electrochemistry for Materials Science, Elsevier, 2008.
- [19] Y. Yao, S. Yao, L. Zhang, H. Wang, Mater. Lett. 61 (2007) 67.
- [20] B.M. Praveen, T.V. Venkatesha, J. Alloys Compd. 482 (2009) 53.
- [21] H.Y. Zheng, M.Z. An, J. Alloys Compd. 459 (2008) 548.
- [22] H. Ataee-Esfahani, M.R. Vaezi, L. Nikzada, B. Yazdani, S.K. Sadrnezhad, J. Alloys Compd. 484 (2009) 540.
- [23] B.R. Tian, Y.F. Cheng, Electrochim. Acta 53 (2007) 511.
- [24] M. Srivastava, V.K.W. Grips, K.S. Rajam, J. Appl. Electrochem. 38 (2008) 669.
- [25] L. Shi, C. Sun, P. Gao, F. Zhou, W. Liu, Appl. Surf. Sci. 252 (2006) 3591.
- [26] M. Srivastava, V.K. William Grips, K.S. Rajam, Appl. Surf. Sci. 253 (2007) 3814.
- [27] B. Bahadormanesh, A. Dolati, J. Alloys Compd. 504 (2010) 514.
- [28] Y. Yang, Y.F. Cheng, Surf. Coat. Technol. 205 (2011) 3198.
- [29] M. Srivastava, V.K. William Grips, A. Jain, K.S. Rajam, Surf. Coat. Technol. 202 (2007) 310.
- [30] Q. Feng, T. Li, H. Teng, X. Zhang, Y. Zhang, C. Liu, J. Jin, Surf. Coat. Technol. 202 (2008) 4137.
- [31] M. Surender, R. Balasubramaniam, B. Basu, Surf. Coat. Technol. 187 (2004) 93.
- [32] A.A. Aal, Mater. Sci. Eng., A 474 (2008) 181.
- [33] M.R. Vaezi, S.K. Sadrnezhad, L. Nikzad, Colloids Surf., A 315 (2008) 176.
- [34] X.H. Chen, C.S. Chen, H.N. Xiao, F.Q. Cheng, G. Zhang, G.J. Yi, Surf. Coat. Technol. 191 (2005) 351.
- [35] L. Wang, Y. Gao, Q. Xue, H. Liu, T. Xu, Appl. Surf. Sci. 242 (2005) 326.
- [36] X. Yang, Q. Li, S. Zhang, H. Gao, F. Luo, Y. Dai, J. Solid State Electrochem. (2010) 1601.
- [37] M. Srivastava, V.E. Selvi, V.K.W. Grips, K.S. Rajam, Surf. Coat. Technol. 201 (2006) 3051.
- [38] Y. Xiu-ying, L. Kang-ju, P. Xiao, W. Fu-hui, Trans. Nonferrous Met. Soc. 19 (2009) 119.
- [39] C.S. Lin, K.C. Huang, J. Appl. Electrochem. 34 (2004) 1013.
- [40] A. Hovestad, L.J.J. Janssen, J. Appl. Electrochem. 25 (1995) 519.
- [41] Q. Jiang, H.M. Lu, Surf. Sci. Rep. 63 (2008) 427.
- [42] B. Bakhit, Production and corrosion behavior of electrodeposited Ni–M/SiC nanocomposite coatings, M.Sc. Thesis, Sahand University of Technology, Tabriz, Iran, Summer 2010.
- [43] G.E. Dieter, Mechanical Metallurgy, McGraw-Hill Inc, 1988.
- [44] E.A. Pavlatou, M. Stroumbouli, P. Gyftou, N. Spyrellis, J. Appl. Electrochem. 36 (2006) 385.
- [45] A.F. Zimmerman, G. Palumbo, K.T. Aust, U. Erb, Mater. Sci. Eng., A 328 (2002) 137.
- [46] L. Benea, P.L. Bonora, A. Borello, S. Martelli, F. Wenger, P. Pontthiaux, J. Galland, Solid State Ionics 151 (2002) 89.
- [47] S.C. Tjong, H. Chen, Mater. Sci. Eng., R 45 (2004) 1.
- [48] M.A. Meyers, A. Mishra, D.J. Benson, Prog. Mater. Sci. 51 (2006) 427.
- [49] K.S. Kumar, H.V. Swygenhoven, S. Suresh, Acta Mater. 51 (2003) 5743.
- [50] K.S. Kumar, S. Suresh, M.F. Chisholm, J.A. Horton, P. Wang, Acta Mater. 51 (2003) 387.
- [51] H. Conrad, Mater. Sci. Eng., A 341 (2003) 216.
- [52] M. Stern, A.L. Geary, J. Electrochem. Soc. 104 (1957) 56.
- [53] ASM Handbook, Corrosion: Fundamentals, Testing, and Protection, Vol. 13A, ASM International, Materials Park Ohio, 2003.
- [54] J. Edward, Coating and Surface Treatment Systems for Metals; a Comprehensive Guide to Selection, ASM International, 1997.
- [55] J.W. Dini, The Materials Science of Coatings and Substrates, Noyes Publications, 1993.
- [56] T. Rabizadeh, S.R. Allahkaram, Mater. Des. 32 (2011) 133.
- [57] T. Lampke, A. Leopold, D. Dietrich, G. Alisch, B. Wielage, Surf. Coat. Technol. 201 (2006) 3510.